ADVERSARIAL ATTACKS ALREADY TELL THE ANSWER: DIRECTIONAL BIAS-GUIDED TEST-TIME DEFENSE FOR VISION-LANGUAGE MODELS

Anonymous authors
Paper under double-blind review

ABSTRACT

Vision-Language Models (VLMs), such as CLIP, have shown strong zero-shot generalization but remain highly vulnerable to adversarial perturbations, posing serious risks in real-world applications. Test-time defenses for VLMs have recently emerged as a promising and efficient approach to defend against adversarial attacks without requiring costly large-scale retraining. In this work, we uncover a surprising phenomenon: under diverse input transformations, adversarial images in CLIP's feature space consistently shift along a dominant direction, in contrast to the dispersed patterns of clean images. We hypothesize that this dominant shift, termed the Defense Direction, opposes the adversarial shift, pointing features back toward their correct class centers. Building on this insight, we propose **Directional Bias-guided Defense (DBD)**, a test-time framework that estimates the Defense Direction and employs a DB-score–based two-stream reconstruction strategy to recover robust representations. Experiments on 15 datasets demonstrate that DBD not only achieves SOTA adversarial robustness while preserving clean accuracy, but also reveals the counterintuitive result that robust accuracy can even surpass clean accuracy. This demonstrates that adversarial perturbations inherently encode directional priors about the true decision boundary.

1 INTRODUCTION

Vision-Language Models (VLMs) such as CLIP (Radford et al., 2021), pre-trained on large-scale image-text pairs, enable strong cross-modal understanding and zero-shot generalization, and are now widely applied across vision and multimodal tasks (Zhang et al., 2024b). Despite its success, CLIP is highly vulnerable to adversarial perturbations: even imperceptible input distortions (Szegedy et al., 2013) can cause severe prediction errors. Such fragility poses critical safety risks in security-sensitive applications, making adversarial robustness a key challenge for reliable deployment.

Adversarial training (Madry et al., 2017; Zhang et al., 2019) is a well-studied strategy for improving model robustness. When extended to VLMs like CLIP, methods such as Adversarial Fine-Tuning (Mao et al., 2022; Wang et al., 2024; Schlarmann et al., 2024) and Adversarial Prompt Tuning (Li et al., 2024; Zhou et al., 2024) have achieved notable progress in strengthening adversarial resistance. However, these approaches rely on task-specific annotated datasets, making training costly and less accessible. Optimization on limited data may also weaken generalization and zero-shot transferability. To address these limitations, recent studies have explored test-time defenses that require no additional training, broadly categorized as prompt-based and transformation-based approaches. Prompt-based defenses (Sheng et al., 2025; Wang et al., 2025) adapt textual prompts for each instance, effectively mitigating attacks but substantially increasing inference latency. Transformation-based methods, such as counterattack perturbation (Xing et al., 2025) and Gaussian noise injection (Tong et al., 2025), offer a simple and efficient way to enhance adversarial robustness by modifying inputs, yet they may degrade performance on clean images.

Given their effectiveness and computational efficiency, transformation-based methods have emerged as a promising approach for test-time defense. Prior studies (Guo et al., 2017; Cohen et al., 2019; Dziugaite et al., 2016; Xie et al., 2017) have shown that various image transformations can mitigate adversarial effects. However, the underlying mechanism of how and why the adversarial effects

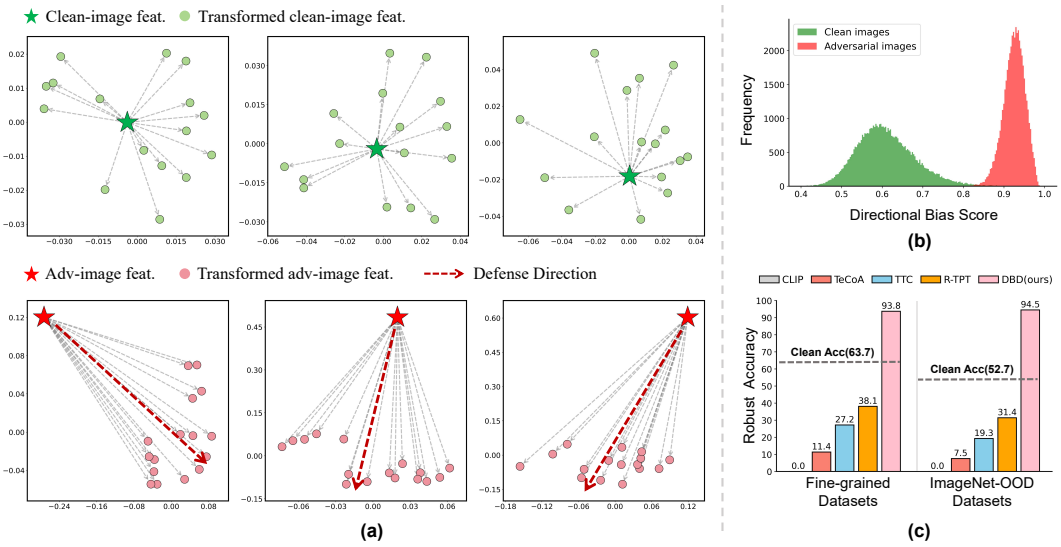

Figure 1: **Illustration of the proposed Directional Bias (DB) analysis:** (a) Visualization of image features under various transformations for clean (first row) and adversarial (second row) inputs, obtained via Multidimensional Scaling (MDS) with $1-$cosine similarity as the distance metric. Clean inputs yield dispersed feature patterns, whereas adversarial inputs exhibit strong directional bias. (b) Histogram of DB-scores on ImageNet, showing clear separation between clean and adversarial images. (c) Comparison of average robust accuracy across multiple methods on ten fine-grained datasets (left) and five ImageNet-OOD datasets (right). Our DBD consistently surpasses previous SOTA methods and even outperforms clean accuracy across all datasets. Adversarial images are generated using 100-step PGD (ℓ_∞, $\epsilon = 4/255$, step size $1/255$) on CLIP-ViT-B/32.

are alleviated remains unexplored, limiting further progress in defense design. To address this, we analyze the latent feature space to investigate how diverse transformations alter image features and thereby mitigate adversarial effects. As shown in Fig. 1(a), when applying various transformations to an input image, the transformed features of a clean image tend to scatter around the original feature, whereas those of an adversarial image consistently shift toward a specific direction, presenting a skewed pattern. To quantify this phenomenon, we further introduce a **Directional Bias (DB) score** to measure the directional concentration of transformed features. As shown in Fig. 1(b), the DB-score exhibits a clear bimodal distribution, effectively distinguishing adversarial from clean ones, as adversarial images consistently exhibit high and concentrated scores.

The above observation prompts a key question: *what does the direction of transformed features represent?* Recall that adversarial attacks work by shifting features away from original class centers, thereby inducing misclassification. We therefore hypothesize that this dominant direction could be anti-parallel to the adversarial shift, pointing features back toward their correct class centers. Building on this insight, we propose **Directional Bias-guided Defense (DBD)**, a test-time framework for VLMs that leverages this specific direction, referred to as **Defense Direction**, to uncover discriminative features. To capture robust Defense Direction, DBD applies a wide range of transformations across spatial, pixel, and frequency domains to obtain diverse augmented features, and then uses entropy-based filtering to retain high-quality ones. Leveraging the DB-score to distinguish between adversarial and clean inputs, we propose a two-stream feature reconstruction strategy to enhance test-time defense: for high DB-score examples, adversarial features are linearly shifted along the Defense Direction to restore correct representations; while for low DB-score examples, the average transformed features are used as test-time augmentation for stabilizing representations.

We conduct extensive experiments across ten fine-grained classification datasets and five ImageNet-OOD datasets. The results demonstrate that our method not only preserves performance on clean images but also achieves substantial improvements over previous state-of-the-art defenses on adversarial examples across all datasets. Remarkably, as shown in Fig. 1(c), the classification accuracy on adversarial images even surpasses that on clean images. *This counterintuitive result justifies that the generation of adversarial examples guided by ground-truth labels implicitly encodes directional priors about the true decision boundary, which we exploit to achieve effective defense.*

Our main contributions are as follows: (1) To the best of our knowledge, we are the first to show that adversarial perturbations implicitly encode directional priors of the true decision boundary, which can be reliably estimated using multiple transformations. (2) We propose Directional Bias-guided Defense (DBD), a test-time framework that leverages these directional priors through Defense Direction estimation and a two-stream reconstruction strategy based on the proposed DB-score, enabling effective and efficient defense. (3) We validate DBD on 15 datasets, demonstrating superior adversarial robustness while preserving zero-shot performance on clean images. In some cases, our method even surpasses the performance on clean images when evaluated on adversarial images.

2 Related Works

Vision-Language Models (VLMs). CLIP (Radford et al., 2021), trained on large-scale image-text pairs, has become a cornerstone vision-language model (VLM) with strong zero-shot generalization and cross-modal reasoning (Zhang et al., 2024b). Building on this paradigm, ALIGN (Jia et al., 2021) and BLIP-2 (Li et al., 2023) further scale or refine the alignment of image-text pairs, while LLaVA (Liu et al., 2023) extends VLMs toward instruction-following and conversational tasks. By aligning modalities in a shared embedding space, these models provide powerful task-agnostic representations. However, prior studies (Zhao et al., 2023; Schlarmann & Hein, 2023) have shown that VLMs are highly vulnerable to adversarial attacks, posing a critical barrier to their deployment in safety-sensitive applications.

Adversarial Attacks and Defenses. Adversarial perturbations are small but carefully crafted input distortions that can drastically mislead deep neural networks (Szegedy et al., 2013). Early works proposed gradient-based attacks such as FGSM (Goodfellow et al., 2014), iterative methods like PGD (Madry et al., 2017), and optimization-based approaches such as CW (Carlini & Wagner, 2017). More recent efforts have introduced adaptive attacks such as AutoAttack (AA) (Croce & Hein, 2020b), a robust benchmark combining four attacks: the score-based black-box Square (Andriushchenko et al., 2020), the minimal-ℓ_p-perturbation FAB (Croce & Hein, 2020a), APGD-CE (using cross-entropy loss), and APGD-DLR (using difference-of-logits-ratio loss). To counter adversarial threats, defenses have been extensively explored. Adversarial training (Madry et al., 2017; Zhang et al., 2019; Shafahi et al., 2019; Wong et al., 2020) optimizes models on perturbed examples to enhance robustness. Input purification (Guo et al., 2017; Xie et al., 2017) transforms inputs toward the clean distribution. Recent diffusion-based purification methods (Nie et al., 2022; Chung et al., 2022) show promise in removing perturbations but often incur high computational cost.

Adversarial Robustness of VLMs. For VLMs such as CLIP, several extensions of adversarial training (Mao et al., 2022; Wang et al., 2024; Schlarmann et al., 2024; Li et al., 2024; Zhou et al., 2024) have been proposed to enhance robustness. TeCoA (Mao et al., 2022) examines the effect of fine-tuning and visual prompt tuning on the zero-shot adversarial robustness of VLMs. Adversarial Prompt Tuning methods, including APT (Li et al., 2024) and AdvPT (Zhang et al., 2024a), focus on optimizing textual prompts without modifying model parameters. However, these methods rely on annotated data and may weaken generalization, motivating test-time defenses that require no additional training. Prompt-based test-time methods such as R-TPT (Sheng et al., 2025) and TAPT (Wang et al., 2025) adapt prompts on a per-instance basis, achieving reasonable robustness at the cost of substantial inference overhead. Transformation-based methods mitigate adversarial attacks by modifying input images. For example, TTC (Xing et al., 2025) generates counterattack perturbations for adversarial images, and AOM (Tong et al., 2025)injects Gaussian noise into inputs. These approaches can improve robustness in practice but often degrade performance on clean images. Our method exploits directional bias in latent feature space to reconstruct features under diverse transformations, enhancing adversarial robustness while preserving clean performance, and achieving an efficient balance between robustness and computational cost.

3 Method

3.1 Preliminaries

Zero-shot classification of CLIP. CLIP (Radford et al., 2021) is a VLM that projects images and texts into a shared embedding space and measures their relationships using cosine similarity. For

zero-shot classification, CLIP consists of two pre-trained encoders: a visual encoder $\mathcal{E}_v$ and a text encoder $\mathcal{E}_t$. For an C-class classification task, given an image x_{test} and a set of class names with prompts $T_c, c \in [1, C]$, CLIP computes text features: $\boldsymbol{f}_{t_c} = \mathcal{E}_t(T_c)$, for each class c, and image feature $\boldsymbol{f}_v = \mathcal{E}_v(x_{test})$. The prediction probability for class c is calculated as:

$$P_{\text{CLIP}}(y = c \mid x_{\text{test}}) = \frac{\exp(\cos(\boldsymbol{f}_{t_c}, \boldsymbol{f}_v)/t)}{\sum_{c'=1}^{C} \exp(\cos(\boldsymbol{f}_{t_{c'}}, \boldsymbol{f}_v)/t)}, \tag{1}$$

where $\cos(\cdot, \cdot)$ is the cosine similarity between the features, and t is a temperature parameter that controls the sharpness of the distribution. The final classification decision is determined by selecting the class with the highest probability:

$$\hat{y} = \arg\max_{c \in [1,C]} P_{\text{CLIP}}(y = c \mid x_{\text{test}}), \tag{2}$$

where $\hat{y}$ represents the predicted class label.

Adversarial attacks for CLIP. Despite its strong zero-shot performance, CLIP is particularly sensitive to small adversarial perturbations (Szegedy et al., 2013). Following recent SOTA test-time method R-TPT (Sheng et al., 2025), we consider a threat model where the attacker has full access to the vanilla CLIP model, but no knowledge of the defense mechanism. This reflects real-world deployment: foundation models like CLIP have publicly available weights, while test-time defenses are typically deployed privately. In this setting, adversarial examples are crafted against CLIP as:

$$\delta = \arg\max_{\delta'} \mathcal{L}(\text{CLIP}(x + \delta', T), y), \quad \text{s.t. } \|\delta'\|_p \leq \epsilon, \tag{3}$$

where y is the ground-truth label of input image x, T is a set of class names with prompts, $\mathcal{L}$ is a loss function (typically cross-entropy loss), and ϵ is the attack budget controlling the magnitude of perturbations to remain imperceptible.

3.2 DBD FOR VLMS

We propose Directional Bias-guided Defense (DBD), a test-time framework for defending VLMs against adversarial attacks. The core idea of DBD is to leverage multiple input transformations to construct diverse reference features, analyze their directional bias relative to the original features, and use this property to guide feature reconstruction. The overall framework consists of three main components: input transformations & feature filtering, Directional Bias (DB) computation, and two-stream feature reconstruction, as illustrated in Fig. 2.

Image Transformations & Feature Filtering. Since individual transformations have inherent drawbacks, relying on a single transformation may produce unreliable features. For example, random cropping is stochastic and may capture mostly background, while filtering can excessively blur important details. To improve robustness, we apply a diverse set of transformations to generate multiple feature candidates, which leverages complementary strengths across transformations to both preserve task-relevant information and disrupt adversarial noise.

We construct an image transformation library covering diverse transformations across three domains: (1) *Spatial domain*: including random cropping, scaling, and flipping. These geometric operations alter object position, size, and orientation, thereby disrupting the structured alignment of adversarial perturbations and weakening their effect. (2) *Pixel domain*: including bit-depth compression (quantization), JPEG compression-decompression, and additive Gaussian noise. These pixel-level modifications distort or overwrite fine-grained perturbations, making them less effective in misleading the model. (3) *Frequency domain*: including Gaussian, mean, and median filtering. By smoothing or suppressing high-frequency components, these filters reduce adversarial noise while largely preserving the semantic content of the image.

Transformed features exhibit varying quality across different transformations, so we apply a feature filtering step to select the most informative and reliable representations. Following common practice in test-time adaptation (Shu et al., 2022), we use the entropy of the model's prediction as a quality

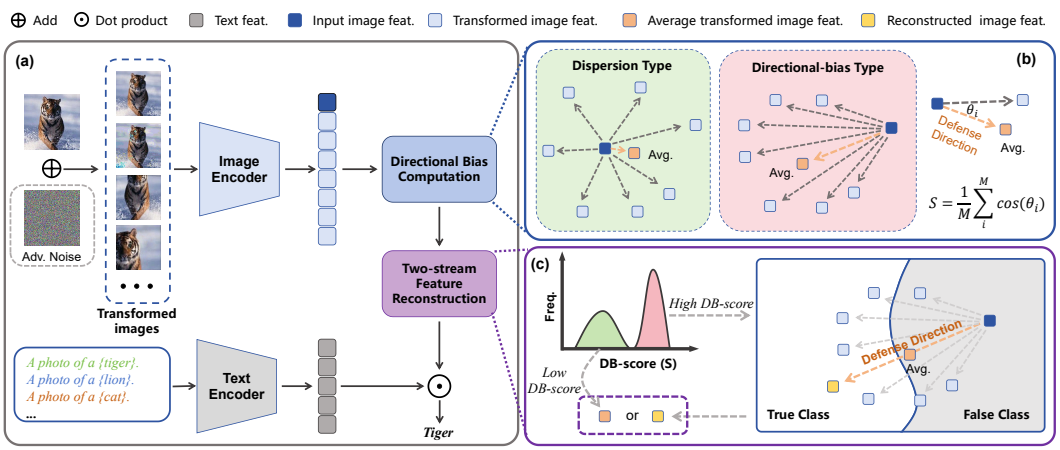

Figure 2: **Overview of the proposed Directional Bias-guided Defense (DBD).** (a) Framework: multiple transformations are applied to the input image, and high-quality transformed features are retained by entropy-based filtering; then the Defense Direction and DB-score are computed for feature reconstruction and classification. (b) Directional Bias (DB) Computation: the Defense Direction is defined from the original feature to the average transformed feature, and the DB-score is the mean cosine similarity between the Defense Direction and each individual displacement vector. (c) Two-stream Feature Reconstruction: for high DB-score (likely adversarial images), the original features are shifted further along the Defense Direction to obtain more robust representations; for low DB-score (likely clean images), the average transformed features are used as test-time augmentation for stabilizing representations.

metric. Specifically, given n transformed images, we pre-compute their features $\boldsymbol{f}_i (i = 1, 2, ..., n)$ and classification probabilities with CLIP, then calculate the entropy for each:

$$E_i = -\sum_c p_{i,c} \log p_{i,c}, \tag{4}$$

where $p_{i,c}$ denotes the predicted probability of the i-th transformed image feature for class c. We then select the k transformed image features with the lowest entropy as high-quality features for subsequent processing:

$$\mathcal{F}_{\text{ref}} = \{\boldsymbol{f}_i \mid i \in \mathcal{I}_k\}, \quad \mathcal{I}_k = \underset{i \subset \{1,\ldots,n\}, |i|=k}{\arg\min} \sum_{j \in i} E_j. \tag{5}$$

Directional Bias (DB) Computation. After applying multiple transformations and feature filtering, we obtain a set of high-quality transformed image features. Visualization (Fig. 1(a)) shows that for clean images, the transformed features exhibit a dispersed pattern around the original feature. In contrast, for adversarial inputs, they consistently shift toward a specific direction, presenting a directional bias pattern. This occurs because transformations partially mitigate adversarial perturbations, aligning the features closer to the clean feature distribution.

Given a set of transformed features $\mathcal{F}_{\text{ref}} = \{\boldsymbol{f}_i \mid i = 1, \ldots, k\}$ and the original feature $\boldsymbol{f}_0$, we define the direction vectors for each transformed feature $\boldsymbol{f}_i$ as unit vectors $\boldsymbol{d}_i = (\boldsymbol{f}_i - \boldsymbol{f}_0)/\|\boldsymbol{f}_i - \boldsymbol{f}_0\|_2$, and compute the Defense Direction $\boldsymbol{d}_{\text{def}}$ as

$$\bar{\boldsymbol{d}} = \frac{1}{k}\sum_{i=1}^{k}(\boldsymbol{f}_i - \boldsymbol{f}_0), \quad \boldsymbol{d}_{\text{def}} = \frac{\bar{\boldsymbol{d}}}{\|\bar{\boldsymbol{d}}\|_2}, \tag{6}$$

where $\|\cdot\|_2$ denotes the ℓ_2 norm (Euclidean distance). The DB-score is computed as the average cosine similarity between each direction and the Defense Direction:

$$S_{\text{db}} = \frac{1}{k}\sum_{i=1}^{k}\langle \boldsymbol{d}_i, \boldsymbol{d}_{\text{def}} \rangle, \tag{7}$$

where $\langle \cdot, \cdot \rangle$ denotes the inner product. As shown in Fig. 1(b), the DB-score exhibits a clear bimodal distribution for clean and adversarial images, allowing simple thresholding to separate them.

Two-stream Feature Reconstruction. Adversarial perturbations shift image features away from the true classification region, thereby inducing misclassification. Intuitively, the Defense Direction $\boldsymbol{d}_{\text{def}}$ could be anti-parallel to the adversarial shift, pointing features back toward their correct classification region. Guided by this intuition, we reconstruct more robust features by linearly shifting the input feature along the Defense Direction. However, due to stochasticity or imperfections in the transformations, the computed Defense Direction may be inaccurate. To reduce the negative impact of inaccurate Defense Direction, we propose a two-stream reconstruction strategy based on the DB-score: (1) High DB-score stream: a high S_{db} indicates a likely adversarial image and a more reliable Defense Direction. In this case, we shift the feature along the Defense Direction to enhance its distinction from the original. (2) Low DB-score stream: a low S_{db} suggests a likely clean image with less reliable direction. For these examples, we use the average of transformed features as test-time augmentation for stabilizing representations. Formally, we introduce a threshold τ on DB-score S_{db}:

$$\hat{\boldsymbol{f}} = \boldsymbol{f}_0 + l \cdot \boldsymbol{d}_{\text{def}}, \quad l = \begin{cases} \|\bar{\boldsymbol{d}}\|_2, & S_{db} \leq \tau \\ \lambda \cdot \|\bar{\boldsymbol{d}}\|_2, & S_{db} > \tau \end{cases}, \tag{8}$$

where $\hat{\boldsymbol{f}}$ is the reconstructed feature and λ is a hyperparameter controlling the magnitude of the feature shift. In practice, we use the distance from the average transformed features to the original feature $\|\bar{\boldsymbol{d}}\|_2$ as a reference for the shift magnitude, which is then scaled by λ. Finally, we use the reconstructed image feature $\hat{\boldsymbol{f}}$ to compute the predicted classification result, as given in Eq.1.

4 Experiments

4.1 Experiment setup

Datasets. Following prior works (Sheng et al., 2025; Li et al., 2024) on the adversarial robustness of CLIP, we evaluate our proposed test-time DBD on ten fine-grained classification datasets and five ImageNet-based out-of-distribution(OOD) benchmarks. The fine-grained datasets span diverse domains: general objects (*Caltech101* (Fei-Fei et al., 2004)), animals (*Pets* (Parkhi et al., 2012)), plants (*Flower102* (Nilsback & Zisserman, 2008)), vehicles (*Cars* (Krause et al., 2013), *Aircraft*) (Maji et al., 2013), textures (*DTD* (Cimpoi et al., 2014)), satellite imagery (*EuroSAT* (Helber et al., 2019)), human actions (*UCF101* (Soomro et al., 2012)), scenes (*SUN397* (Xiao et al., 2010)), and food (*Food101* (Bossard et al., 2014)). For ImageNet-OOD evaluation, we use *ImageNet* (Deng et al., 2009) and four established variants: *ImageNet-A* (Hendrycks et al., 2021b), *ImageNet-V2* (Recht et al., 2019) , *ImageNet-R* (Hendrycks et al., 2021a), and *ImageNet-S* (Wang et al., 2019). Since our method targets test-time adversarial robustness, we do not require access to any training sets.

Implementation details. We use official pre-trained CLIP backbones (ResNet-50 (He et al., 2016), ViT-B/32, and ViT-B/16 (Dosovitskiy et al., 2020)) as the base models. Adversarial images are generated with PGD (Madry et al., 2017) under the L_∞ norm constraint. Following prior works (Sheng et al., 2025; Li et al., 2024), we evaluate two threat levels. For low-strength attack, we use PGD-10 with $\epsilon = 1/255$ on CLIP-ResNet50; for high-strength attack, we use PGD-100 with $\epsilon = 4/255$ on CLIP-ViT-B/32 and CLIP-ViT-B/16. The step size for all attacks is $\alpha = \epsilon/4$. For our DBD, we apply $n = 31$ transformations per input, yielding 32 images including the original, and then select $k = 16$ transformed image features via entropy-based filtering. The DB-score threshold is $\tau = 0.8$, and the feature shift magnitude is set to $\lambda = 2.5$. Both are estimated from ImageNet validation set (50k images). Experiments are conducted in PyTorch on RTX 3090 GPUs.

Baselines. We compare DBD with several existing methods, including adversarial fine-tuning on ImageNet (TeCoA (Mao et al., 2022)), adversarial prompt tuning on downstream datasets with 16 shots (APT (Li et al., 2024)), test-time prompt tuning (R-TPT (Sheng et al., 2025)), test-time input transformation method (TTC (Xing et al., 2025)), and the original CLIP (Radford et al., 2021) models. Except for APT, which uses few-shot tuning , all other methods operate in a zero-shot setting. Baseline results are obtained from official reports or reproduced using official code.

4.2 Main Results

Results on fine-grained datasets. We evaluate the adversarial robustness of DBD on ten fine-grained classification datasets, with results summarized in Table 1. Under the CLIP-ViT-B/32 and

Table 1: Results (%) of clean accuracy (Acc.) and robust accuracy (Rob.) of various defense methods on ten **fine-grained classification datasets**. Robust accuracies are highlighted with gray background. Best clean accuracies are (**bold**), and best robust accuracies are (**bold red**).

Method	Caltech101		Pets		Cars		Flower102		Aircraft		DTD		EuroSAT		UCF101		SUN397		Food101		Avg.	
	Acc.	Rob.	Acc.	Rob.	Acc.	Rob.	Acc.	Rob.	Acc.	Rob.	Acc.	Rob.	Acc.	Rob.	Acc.	Rob.	Acc.	Rob.	Acc.	Rob.	Acc.	Rob.
PGD-10 ($\epsilon = 1/255$) on CLIP-ResNet50																						
CLIP	89.1	2.1	85.0	0.0	57.3	0.0	65.9	0.0	19.6	0.0	**48.5**	0.4	**37.5**	0.0	59.7	0.0	62.7	0.0	**75.6**	0.0	**60.1**	0.3
TeCoA	78.2	64.1	76.2	54.4	24.1	9.2	32.6	17.3	6.6	2.4	30.7	21.4	23.8	19.0	40.4	21.8	38.6	19.7	29.2	12.3	38.1	24.2
R-TPT	86.0	79.9	84.7	73.4	58.4	42.1	60.7	51.0	18.1	12.3	41.1	34.3	21.2	15.8	59.2	50.3	60.8	50.7	73.3	57.8	56.3	46.8
DBD	**90.1**	**98.7**	**86.0**	**95.9**	**60.0**	**86.2**	**65.9**	**88.3**	**21.6**	**56.3**	47.9	**85.2**	29.4	**81.3**	**60.6**	**88.9**	**63.8**	**93.2**	75.0	**97.4**	60.0	**87.1**
PGD-100 ($\epsilon = 4/255$) on CLIP-ViT-B/32																						
CLIP	93.3	0.1	86.6	0.0	61.2	0.0	67.0	0.0	20.6	0.0	49.9	0.0	50.8	0.0	63.6	0.0	65.7	0.0	78.7	0.0	63.7	0.0
TeCoA	81.5	46.1	64.4	16.7	11.5	1.1	30.1	9.5	6.7	0.6	29.3	12.7	13.8	11.1	34.0	6.3	34.7	6.5	22.4	3.0	32.8	11.4
APT	86.6	57.6	66.6	17.2	41.9	9.9	**84.4**	47.0	**28.7**	6.8	47.5	21.4	**67.2**	23.5	58.2	18.9	46.6	10.5	33.3	6.8	56.1	22.0
TTC	89.5	47.6	61.0	41.5	45.9	21.3	65.5	29.2	15.4	11.1	39.5	20.4	44.8	15.4	60.8	27.6	46.3	25.7	74.4	32.2	54.3	27.2
R-TPT	91.0	77.8	84.8	57.7	63.3	28.3	63.3	38.8	19.6	10.1	42.7	29.9	31.9	6.5	63.1	44.2	64.0	44.1	78.5	43.5	60.2	38.1
DBD	**93.8**	**99.0**	**86.8**	**96.2**	**63.7**	**91.2**	68.7	**94.7**	22.4	**66.3**	**51.5**	**88.3**	41.7	**92.6**	**65.3**	**92.2**	**67.1**	**94.2**	**80.1**	**98.4**	**64.1**	**91.3**
PGD-100 ($\epsilon = 4/255$) on CLIP-ViT-B/16																						
CLIP	94.2	0.0	90.3	0.0	66.2	0.0	73.0	0.0	27.1	0.0	53.2	0.0	**55.7**	0.0	67.0	0.0	67.9	0.0	84.2	0.0	**67.9**	0.0
TTC	90.3	16.1	57.9	17.7	57.4	11.3	68.5	19.8	21.7	2.8	41.5	15.3	44.7	0.6	64.8	4.9	51.5	15.7	81.0	21.2	58.0	12.5
R-TPT	93.7	83.1	87.4	63.3	67.0	36.0	68.1	46.4	24.0	14.4	46.6	34.9	34.6	10.2	67.8	47.3	65.7	46.5	84.3	49.7	63.9	43.2
DBD	**94.8**	**99.4**	**90.7**	**97.1**	**67.8**	**93.4**	**73.6**	**97.5**	**29.7**	**71.9**	**54.5**	**92.3**	44.9	**93.3**	**68.2**	**95.9**	**69.0**	**97.4**	**84.7**	**99.5**	67.8	**93.8**

Table 2: Results (%) of clean accuracy (Acc.) and robust accuracy (Rob.) of various defense methods on five **ImageNet-OOD datasets**. Robust accuracies are highlighted with gray background. Best clean accuracies are (**bold**), and best robust accuracies are (**bold red**).

Attack & Model	Method	ImageNet		ImageNet-A		ImageNet-V2		ImageNet-R		ImageNet-S		Avg.	
		Acc.	Rob.	Acc.	Rob.	Acc.	Rob.	Acc.	Rob.	Acc.	Rob.	Acc.	Rob.
PGD-10 ($\epsilon = 1/255$) on CLIP-ResNet50	CLIP	61.5	0.0	23.8	0.0	54.7	0.0	60.0	0.4	35.6	0.3	47.1	0.2
	TeCoA	48.4	28.1	4.9	1.2	39.6	21.7	40.6	25.7	18.3	11.6	30.3	17.7
	R-TPT	60.8	47.3	**28.0**	14.2	54.7	41.6	57.7	46.6	34.0	26.0	47.0	35.1
	DBD	**63.1**	**94.5**	23.0	**89.0**	**55.7**	**93.0**	**63.0**	**94.0**	**38.1**	**73.7**	**48.6**	**88.8**
PGD-100 ($\epsilon = 4/255$) on CLIP-ViT-B/32	CLIP	64.4	0.0	31.1	0.0	57.2	0.0	68.3	0.0	42.5	0.0	52.7	0.0
	TeCoA	39.5	9.7	4.2	0.3	32.4	7.3	38.0	12.7	18.5	7.6	26.5	7.5
	TTC	35.4	25.7	27.5	8.4	41.3	21.4	53.4	28.1	29.8	12.8	37.5	19.3
	R-TPT	64.2	40.4	**36.6**	11.0	58.0	34.3	70.0	47.9	41.7	23.6	54.1	31.4
	DBD	**66.3**	**95.3**	32.9	**95.3**	**59.1**	**94.3**	**71.7**	**98.2**	**45.1**	**89.5**	**55.0**	**94.5**
PGD-100 ($\epsilon = 4/255$) on CLIP-ViT-B/16	CLIP	69.6	0.0	50.6	0.0	63.4	0.0	77.1	0.0	49.1	0.0	62.0	0.0
	TTC	37.8	17.4	46.6	9.9	48.9	16.1	63.3	12.4	38.5	1.9	47.0	11.5
	R-TPT	69.4	46.6	**57.9**	20.7	63.9	40.2	77.0	57.6	47.9	30.3	63.2	39.1
	DBD	**71.1**	**97.7**	52.1	**98.9**	**64.7**	**97.3**	**79.5**	**99.4**	**51.1**	**95.3**	**63.7**	**97.7**

PGD-100 ($\epsilon = 4/255$) setting, the original CLIP model demonstrates strong zero-shot classification performance (63.7%) but is almost entirely vulnerable to adversarial attacks (0.0%). Adversarial fine-tuning (TeCoA) improves defense to 11.4%, but at the cost of reduced zero-shot performance on clean images (63.7% $\rightarrow$ 32.8%). Adversarial prompt tuning (FAP) further enhances robustness (0.0% $\rightarrow$ 22.0%) while mitigating the drop in clean accuracy (63.7% $\rightarrow$ 56.1%), though its few-shot setting introduces data dependency. Test-time input transformation method (TTC) achieves moderate robustness on CLIP-ViT-B/32 (0.0% $\rightarrow$ 27.2%) but are sensitive to model architecture, with only 12.5% on CLIP-ViT-B/16. Previous state-of-the-art test-time prompt tuning method (R-TPT) attains better robustness (0.0% $\rightarrow$ 38.1%) and largely preserves zero-shot performance on clean images (63.7% $\rightarrow$ 60.2%). In contrast, ours DBD maintains zero-shot performance close to the original CLIP across all three backbones (even exceeding it on CLIP-ViT-B/32) and achieves substantially higher robustness on adversarial examples, reaching 93.8% on CLIP-ViT-B/16, significantly surpassing both R-TPT and the performance on clean examples.

Results on ImageNet-OOD datasets. Results on ImageNet-OOD benchmarks are summarized in Table 2. The original CLIP model demonstrates strong robustness to distribution shifts but remains highly vulnerable to adversarial attacks. Notably, our DBD method not only preserves but slightly improves zero-shot classification on clean images (e.g., 52.7% $\rightarrow$ 55.0% on CLIP-ViT-B/32), which we attribute to the combination of diverse image transformations and entropy-based feature filtering that produces more robust and accurate features. Across all three backbones, DBD substantially outperforms the previous state-of-the-art R-TPT on adversarial examples, achieving up to 97.7% on CLIP-ViT-B/16, a performance that even surpasses the classification accuracy on clean examples.

Discussion. *Remarkably, the classification accuracy on adversarial images significantly exceeds that on clean images. This counterintuitive result suggests that the generation of adversarial examples guided by ground-truth labels implicitly encodes directional priors about the true decision boundary. Our method leverages this by applying multiple image transformations to estimate the Defense Direction , then linearly shifting features along it to reconstruct robust representations.*

4.3 More Analysis

Table 3: Robust accuracy (%) under PGD-100 ($\epsilon = 4/255$) on CLIP-ViT-B/16 using **pseudo-labels** across six fine-grained datasets. The last row shows the clean accuracy as a reference.

Method	Caltech101	Pets	Flower102	Aircraft	DTD	UCF101	Avg.
CLIP	1.7	3.1	2.7	1.5	4.2	4.5	2.9
R-TPT	84.1	66.1	49.8	18.2	37.1	52.7	51.3
DBD	**94.1**	**88.6**	**72.3**	**26.3**	**53.1**	**66.5**	**66.8**
Clean	94.2	90.3	73.0	27.2	53.2	67.0	67.5

Analysis under PGD attack with pseudo-label. The previous experiments demonstrate that when PGD generates adversarial examples using ground-truth labels, our method achieves robust accuracy which significantly exceeds clean accuracy. To further validate its effectiveness without relying on ground-truth labels, we consider a pseudo-label setting. Specifically, we use CLIP's own predictions on clean images as pseudo-labels to guide PGD in generating adversarial examples. As shown in Table 3, under this setting the vanilla CLIP model remains highly vulnerable. In contrast, our method consistently outperforms R-TPT and achieves robust accuracy comparable to clean accuracy (e.g., 67.5% $\rightarrow$ 66.8% on CLIP-ViT-B/16). This indicates that our method is able to fully leverage the directional prior information carried by adversarial examples.

Analysis under various attacks. To demonstrate the generality of our method, we evaluate DBD and baseline methods under additional adversarial attacks, including FGSM (Goodfellow et al., 2014), CW (Carlini & Wagner, 2017), AutoAttack (AA) (Croce & Hein, 2020b), and four component attacks of AA: Square Attack (Andriushchenko et al., 2020), targeted FAB (Croce & Hein, 2020a), untargeted APGD-CE, and targeted APGD-DLR. We evaluate various attacks on the same six fine-grained datasets in Table 3, with the results summarized in Table 4. DBD consistently demonstrates robust defense performance across all attack types, significantly outperforming R-TPT. Notably, under AA on CLIP-ViT-B/16, DBD achieves an average robust accuracy of 69.8%, surpassing the average clean accuracy of 67.5%.

Table 4: Average robust accuracy (%) across six fine-grained datasets under **various attacks** on CLIP-ViT-B/16. All attacks are conducted under the ℓ_∞ norm with perturbation budget $\epsilon = 4/255$.

Method	FGSM	CW	AA	FAB	Square	APGD-CE	APGD-DLR	Avg.
CLIP	11.8	1.0	0.0	12.9	11.7	0.1	0.1	5.1
R-TPT	38.9	55.6	45.0	59.5	59.2	45.0	48.8	50.4
DBD	**75.2**	**69.1**	**69.8**	**69.3**	**65.1**	**69.8**	**68.5**	**69.2**

Analysis of inference efficiency. We compare DBD's inference efficiency with baseline methods. Table 5 reports the training time of APT and the inference time of test-time defenses R-TPT, TTC, and DBD on UCF101 using CLIP-ViT-B/32. Training-time defenses incur substantial training costs, while test-time defenses avoid this but increase inference overhead. DBD achieves a favorable balance between robustness and efficiency, outperforming R-TPT in both accuracy and inference speed.

Table 5: Running time and robust accuracies (%) of different defense methods against adversarial attacks on UCF101 dataset using CLIP-ViT-B/32. APT is evaluated with 16 shots, while R-TPT and DBD are evaluated with 32 views.

Method	Stage	Running time	Rob.
APT	Training time	22m47s / 200 epochs	18.9
TTC	Test time	0.008s / image	27.6
R-TPT	Test time	0.181s / image	44.3
DBD	Test time	0.025s / image	**92.2**

4.4 Ablation Study

Ablation of the feature shift magnitude factor λ. To evaluate the impact of the shift magnitude factor λ on the performance of DBD, we test three attack settings across 15 datasets. The average robust accuracy of all is shown in Fig.3(a). When $\lambda = 0$, the reconstructed feature reduces to the original feature, yielding nearly no defense. With $\lambda = 1.0$, the reconstructed feature becomes the average of transformed features, achieving an average robust accuracy of 34.8%. At $\lambda = 2.5$, DBD reaches 92.1% accuracy, demonstrating that linearly shifting the original feature along the Defense Direction reconstructs robust features that align with the correct class. This highlights the reliability of the Defense Direction identified by DBD.

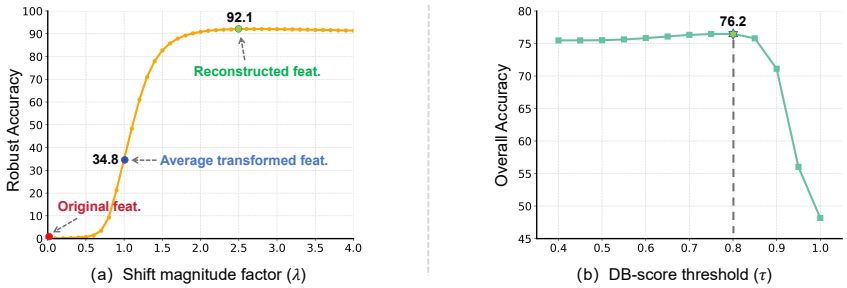

Figure 3: (a) Average robust accuracy (%) across 15 datasets under three attack settings for different values of the feature shift magnitude factor λ. (b) Average overall accuracy (%) for different values of the DB-score threshold τ, computed by averaging both clean and robust accuracies across all datasets and attack settings.

Table 6: **Ablation study.** Results (%) of clean accuracy (Acc.) and robust accuracy (Rob.) are average over 15 datasets and three attack settings. The left five columns correspond to different image transformation types, while the middle two columns represent DBD mechanisms (linear feature shifting and DB-score-based thresholding).

Random Crop-Resize-Flip	Bit-depth Reduction	JPEG Compression	Guassian Noise	Image Filtering	Feature Shift	DB-score Threshold	Acc.	Rob.
-	-	-	-	-	-	-	60.6	0.0
✓	-	-	-	-	✓	-	53.0	91.2
-	✓	-	-	-	✓	-	24.1	82.4
-	-	✓	-	-	✓	-	55.7	88.4
-	-	-	✓	-	✓	-	36.1	85.5
-	-	-	-	✓	✓	-	43.9	87.3
✓	✓	✓	✓	✓	-	-	**61.5**	34.8
✓	✓	✓	✓	✓	✓	-	58.9	**92.1**
✓	✓	✓	✓	✓	✓	✓	61.2	91.7

Ablation of the DB-score threshold τ. DBD employs a DB-score threshold τ to distinguish high-score examples (likely adversarial) from low-score examples (likely clean). We evaluate the effect of τ under three attack settings across 15 datasets, reporting the overall mean accuracy obtained by averaging both clean and adversarial performance across all datasets and attack settings (Fig.3(b)). The results show that setting $\tau = 0.8$ yields the best overall performance. At this threshold, DBD successfully reconstructs robust features for the majority of adversarial images, while simultaneously avoiding inaccurate shifts in most clean examples, thereby achieving a well-balanced trade-off between robust and clean accuracy.

Ablation of DBD mechanisms. We conduct ablation experiments on all DBD components, with results average over 15 datasets and three attack settings (Table 6). Our analysis reveals four key findings: (1) Using a single type of image transformation with feature shifting provides strong adversarial defense but reduces clean image performance. (2) Aggregating multiple transformations without linear shifting gives the best clean accuracy but weak defense. (3) Adding linear shifting on top of multiple transformations substantially improves adversarial robustness, at the cost of some clean performance. (4) Applying the DB-score-based threshold to handle high-score and low-score examples separately achieves the best trade-off between clean accuracy and adversarial robustness.

5 Conclusion

In this work, we found that adversarial examples exhibit a strong directional bias under multiple input transformations, in contrast to the dispersed behavior of clean examples. Building on this observation, we proposed Directional Bias-guided Defense (DBD), a test-time framework that leverages the directional bias to reconstruct robust features through Defense Direction estimation and a two-stream reconstruction strategy based on the proposed DB-score. Experiments on 15 datasets under three attack settings demonstrate that DBD achieves state-of-the-art adversarial robustness while preserving zero-shot performance on clean images. Remarkably, robust accuracy even surpasses clean accuracy, highlighting that adversarial perturbations implicitly encode directional priors about the true decision boundary. We believe that our work sheds light on new perspectives for training-free defenses in VLMs.

REFERENCES

Maksym Andriushchenko, Francesco Croce, Nicolas Flammarion, and Matthias Hein. Square attack: a query-efficient black-box adversarial attack via random search. In *European conference on computer vision*, pp. 484–501. Springer, 2020.

Anish Athalye, Nicholas Carlini, and David Wagner. Obfuscated gradients give a false sense of security: Circumventing defenses to adversarial examples. In *International conference on machine learning*, pp. 274–283. PMLR, 2018.

Lukas Bossard, Matthieu Guillaumin, and Luc Van Gool. Food-101–mining discriminative components with random forests. In *European conference on computer vision*, pp. 446–461. Springer, 2014.

Nicholas Carlini and David Wagner. Towards evaluating the robustness of neural networks. In *2017 ieee symposium on security and privacy (sp)*, pp. 39–57. Ieee, 2017.

Hyungjin Chung, Jeongsol Kim, Michael T Mccann, Marc L Klasky, and Jong Chul Ye. Diffusion posterior sampling for general noisy inverse problems. *arXiv preprint arXiv:2209.14687*, 2022.

Mircea Cimpoi, Subhransu Maji, Iasonas Kokkinos, Sammy Mohamed, and Andrea Vedaldi. Describing textures in the wild. In *Proc. CVPR*, 2014.

Jeremy Cohen, Elan Rosenfeld, and Zico Kolter. Certified adversarial robustness via randomized smoothing. In *international conference on machine learning*, pp. 1310–1320. PMLR, 2019.

Francesco Croce and Matthias Hein. Minimally distorted adversarial examples with a fast adaptive boundary attack. In *International conference on machine learning*, pp. 2196–2205. PMLR, 2020a.

Francesco Croce and Matthias Hein. Reliable evaluation of adversarial robustness with an ensemble of diverse parameter-free attacks. In *ICML*, 2020b.

Jia Deng, Wei Dong, Richard Socher, Li-Jia Li, Kai Li, and Li Fei-Fei. Imagenet: A large-scale hierarchical image database. In *Proc. CVPR*, 2009.

Alexey Dosovitskiy, Lucas Beyer, Alexander Kolesnikov, Dirk Weissenborn, Xiaohua Zhai, Thomas Unterthiner, Mostafa Dehghani, Matthias Minderer, Georg Heigold, Sylvain Gelly, et al. An image is worth 16x16 words: Transformers for image recognition at scale. *arXiv preprint arXiv:2010.11929*, 2020.

Gintare Karolina Dziugaite, Zoubin Ghahramani, and Daniel M Roy. A study of the effect of jpg compression on adversarial images. *arXiv preprint arXiv:1608.00853*, 2016.

Li Fei-Fei, Rob Fergus, and Pietro Perona. Learning generative visual models from few training examples: An incremental bayesian approach tested on 101 object categories. In *Proc. CVPR Workshops*, 2004.

Ian J Goodfellow, Jonathon Shlens, and Christian Szegedy. Explaining and harnessing adversarial examples. *arXiv preprint arXiv:1412.6572*, 2014.

Chuan Guo, Mayank Rana, Moustapha Cisse, and Laurens Van Der Maaten. Countering adversarial images using input transformations. *arXiv preprint arXiv:1711.00117*, 2017.

Kaiming He, Xiangyu Zhang, Shaoqing Ren, and Jian Sun. Deep residual learning for image recognition. In *Proceedings of the IEEE conference on computer vision and pattern recognition*, pp. 770–778, 2016.

Patrick Helber, Benjamin Bischke, Andreas Dengel, and Damian Borth. Eurosat: A novel dataset and deep learning benchmark for land use and land cover classification. *IEEE Journal of Selected Topics in Applied Earth Observations and Remote Sensing*, 12(7):2217–2226, 2019.

Dan Hendrycks, Steven Basart, Norman Mu, Saurav Kadavath, Frank Wang, Evan Dorundo, Rahul Desai, Tyler Zhu, Samyak Parajuli, Mike Guo, et al. The many faces of robustness: A critical analysis of out-of-distribution generalization. In *Proc. ICCV*, 2021a.

Dan Hendrycks, Kevin Zhao, Steven Basart, Jacob Steinhardt, and Dawn Song. Natural adversarial examples. In *Proc. CVPR*, 2021b.

Chao Jia, Yinfei Yang, Ye Xia, Yi-Ting Chen, Zarana Parekh, Hieu Pham, Quoc V. Le, Yunhsuan Sung, Zhen Li, and Tom Duerig. Scaling up visual and vision-language representation learning with noisy text supervision, 2021. URL https://arxiv.org/abs/2102.05918.

Hoki Kim. Torchattacks: A pytorch repository for adversarial attacks. *arXiv preprint arXiv:2010.01950*, 2020.

Jonathan Krause, Michael Stark, Jia Deng, and Li Fei-Fei. 3d object representations for fine-grained categorization. In *Proc. ICCV Workshops*, 2013.

Junnan Li, Dongxu Li, Silvio Savarese, and Steven Hoi. Blip-2: Bootstrapping language-image pre-training with frozen image encoders and large language models. In *International conference on machine learning*, pp. 19730–19742. PMLR, 2023.

Lin Li, Haoyan Guan, Jianing Qiu, and Michael Spratling. One prompt word is enough to boost adversarial robustness for pre-trained vision-language models. In *Proceedings of the IEEE/CVF Conference on Computer Vision and Pattern Recognition*, pp. 24408–24419, 2024.

Haotian Liu, Chunyuan Li, Qingyang Wu, and Yong Jae Lee. Visual instruction tuning, 2023.

Aleksander Madry, Aleksandar Makelov, Ludwig Schmidt, Dimitris Tsipras, and Adrian Vladu. Towards deep learning models resistant to adversarial attacks. *arXiv preprint arXiv:1706.06083*, 2017.

Subhransu Maji, Esa Rahtu, Juho Kannala, Matthew Blaschko, and Andrea Vedaldi. Fine-grained visual classification of aircraft. *arXiv preprint arXiv:1306.5151*, 2013.

Chengzhi Mao, Scott Geng, Junfeng Yang, Xin Wang, and Carl Vondrick. Understanding zero-shot adversarial robustness for large-scale models. *arXiv preprint arXiv:2212.07016*, 2022.

Weili Nie, Brandon Guo, Yujia Huang, Chaowei Xiao, Arash Vahdat, and Anima Anandkumar. Diffusion models for adversarial purification. *arXiv preprint arXiv:2205.07460*, 2022.

Maria-Elena Nilsback and Andrew Zisserman. Automated flower classification over a large number of classes. In *Proc. ICVGIP*, 2008.

Omkar M Parkhi, Andrea Vedaldi, Andrew Zisserman, and CV Jawahar. Cats and dogs. In *Proc. CVPR*, 2012.

Sarah Pratt, Ian Covert, Rosanne Liu, and Ali Farhadi. What does a platypus look like? generating customized prompts for zero-shot image classification. In *Proceedings of the IEEE/CVF international conference on computer vision*, pp. 15691–15701, 2023.

Alec Radford, Jong Wook Kim, Chris Hallacy, Aditya Ramesh, Gabriel Goh, Sandhini Agarwal, Girish Sastry, Amanda Askell, Pamela Mishkin, Jack Clark, et al. Learning transferable visual models from natural language supervision. In *International conference on machine learning*, pp. 8748–8763. PmLR, 2021.

Benjamin Recht, Rebecca Roelofs, Ludwig Schmidt, and Vaishaal Shankar. Do imagenet classifiers generalize to imagenet? In *Proc. ICML*, 2019.

Christian Schlarmann and Matthias Hein. On the adversarial robustness of multi-modal foundation models. In *Proceedings of the IEEE/CVF International Conference on Computer Vision*, pp. 3677–3685, 2023.

Christian Schlarmann, Naman Deep Singh, Francesco Croce, and Matthias Hein. Robust clip: Unsupervised adversarial fine-tuning of vision embeddings for robust large vision-language models. *arXiv preprint arXiv:2402.12336*, 2024.

Ali Shafahi, Mahyar Najibi, Mohammad Amin Ghiasi, Zheng Xu, John Dickerson, Christoph Studer, Larry S Davis, Gavin Taylor, and Tom Goldstein. Adversarial training for free! *Advances in neural information processing systems*, 32, 2019.

Lijun Sheng, Jian Liang, Zilei Wang, and Ran He. R-tpt: Improving adversarial robustness of vision-language models through test-time prompt tuning. In *Proceedings of the Computer Vision and Pattern Recognition Conference*, pp. 29958–29967, 2025.

Manli Shu, Weili Nie, De-An Huang, Zhiding Yu, Tom Goldstein, Anima Anandkumar, and Chaowei Xiao. Test-time prompt tuning for zero-shot generalization in vision-language models. *Advances in Neural Information Processing Systems*, 35:14274–14289, 2022.

Khurram Soomro, Amir Roshan Zamir, and Mubarak Shah. A dataset of 101 human action classes from videos in the wild. *Center for Research in Computer Vision*, 2(11):1–7, 2012.

Christian Szegedy, Wojciech Zaremba, Ilya Sutskever, Joan Bruna, Dumitru Erhan, Ian Goodfellow, and Rob Fergus. Intriguing properties of neural networks. *arXiv preprint arXiv:1312.6199*, 2013.

Baoshun Tong, Hanjiang Lai, Yan Pan, and Jian Yin. On the zero-shot adversarial robustness of vision-language models: A truly zero-shot and training-free approach. In *Proceedings of the Computer Vision and Pattern Recognition Conference*, pp. 19921–19930, 2025.

Haohan Wang, Songwei Ge, Zachary Lipton, and Eric P Xing. Learning robust global representations by penalizing local predictive power. In *Proc. NeurIPS*, 2019.

Sibo Wang, Jie Zhang, Zheng Yuan, and Shiguang Shan. Pre-trained model guided fine-tuning for zero-shot adversarial robustness. In *Proceedings of the IEEE/CVF conference on computer vision and pattern recognition*, pp. 24502–24511, 2024.

Xin Wang, Kai Chen, Jiaming Zhang, Jingjing Chen, and Xingjun Ma. Tapt: Test-time adversarial prompt tuning for robust inference in vision-language models. In *Proceedings of the Computer Vision and Pattern Recognition Conference*, pp. 19910–19920, 2025.

Eric Wong, Leslie Rice, and J Zico Kolter. Fast is better than free: Revisiting adversarial training. *arXiv preprint arXiv:2001.03994*, 2020.

Jianxiong Xiao, James Hays, Krista A Ehinger, Aude Oliva, and Antonio Torralba. Sun database: Large-scale scene recognition from abbey to zoo. In *2010 IEEE computer society conference on computer vision and pattern recognition*, pp. 3485–3492. IEEE, 2010.

Cihang Xie, Jianyu Wang, Zhishuai Zhang, Zhou Ren, and Alan Yuille. Mitigating adversarial effects through randomization. *arXiv preprint arXiv:1711.01991*, 2017.

Songlong Xing, Zhengyu Zhao, and Nicu Sebe. Clip is strong enough to fight back: Test-time counterattacks towards zero-shot adversarial robustness of clip. In *Proceedings of the Computer Vision and Pattern Recognition Conference*, pp. 15172–15182, 2025.

Hongyang Zhang, Yaodong Yu, Jiantao Jiao, Eric Xing, Laurent El Ghaoui, and Michael Jordan. Theoretically principled trade-off between robustness and accuracy. In *International conference on machine learning*, pp. 7472–7482. PMLR, 2019.

Jiaming Zhang, Xingjun Ma, Xin Wang, Lingyu Qiu, Jiaqi Wang, Yu-Gang Jiang, and Jitao Sang. Adversarial prompt tuning for vision-language models. In *European conference on computer vision*, pp. 56–72. Springer, 2024a.

Jingyi Zhang, Jiaxing Huang, Sheng Jin, and Shijian Lu. Vision-language models for vision tasks: A survey. *IEEE transactions on pattern analysis and machine intelligence*, 46(8):5625–5644, 2024b.

Yunqing Zhao, Tianyu Pang, Chao Du, Xiao Yang, Chongxuan Li, Ngai-Man Man Cheung, and Min Lin. On evaluating adversarial robustness of large vision-language models. *Advances in Neural Information Processing Systems*, 36:54111–54138, 2023.

Yiwei Zhou, Xiaobo Xia, Zhiwei Lin, Bo Han, and Tongliang Liu. Few-shot adversarial prompt learning on vision-language models. *Advances in Neural Information Processing Systems*, 37: 3122–3156, 2024.

A APPENDIX

A.1 ALGORITHM

We provide a detailed pseudocode of our proposed DBD in Algorithm 1.

Algorithm 1: Directional Bias-guided Defense (DBD) for VLMs

Input: Input image x, pre-trained CLIP vision encoder $\mathcal{E}_v$, classification head $\mathcal{H}$, transformation library $\mathcal{T}$, DB threshold τ, shift factor λ

Output: Robust feature $\hat{\boldsymbol{f}}$ and classification result y

Step 1: Image Transformations & Feature Filtering

for *transformation* $t \in \mathcal{T}$ **do**
- $x_t \leftarrow t(x)$; `// Apply transformation`
- $\boldsymbol{f}_t \leftarrow \mathcal{E}_v(x_t)$; `// Extract feature`
- $p_t \leftarrow \mathcal{H}(\boldsymbol{f}_t)$; `// Compute classification probabilities`
- $E_t \leftarrow -\sum_c p_{t,c} \log p_{t,c}$; `// Compute entropy`

$\mathcal{F}_{\text{ref}} \leftarrow k$ features with lowest E_t

Step 2: Directional Bias Computation

$\boldsymbol{f}_0 \leftarrow \mathcal{E}_v(x)$; `// Original feature`

for $\boldsymbol{f}_i \in \mathcal{F}_{\text{ref}}$ **do**
- $\boldsymbol{d}_i \leftarrow (\boldsymbol{f}_i - \boldsymbol{f}_0)/\|\boldsymbol{f}_i - \boldsymbol{f}_0\|_2$; `// Unit displacement vector`

$\bar{\boldsymbol{d}} \leftarrow \frac{1}{k}\sum_{i=1}^{k}(\boldsymbol{f}_i - \boldsymbol{f}_0)$; `// Mean displacement`

$\boldsymbol{d}_{\text{def}} \leftarrow \bar{\boldsymbol{d}}/\|\bar{\boldsymbol{d}}\|_2$; `// Defense Direction`

$S_{\text{db}} \leftarrow \frac{1}{k}\sum_{i=1}^{k}\langle \boldsymbol{d}_i, \boldsymbol{d}_{\text{def}} \rangle$; `// DB-score`

Step 3: Two-stream Feature Reconstruction & Prediction

if $S_{\text{db}} \leq \tau$ **then**
- $\hat{\boldsymbol{f}} \leftarrow \boldsymbol{f}_0 + \|\bar{\boldsymbol{d}}\|_2 \cdot \boldsymbol{d}_{\text{def}}$; `// Likely clean`

else
- $\hat{\boldsymbol{f}} \leftarrow \boldsymbol{f}_0 + \lambda \cdot \|\bar{\boldsymbol{d}}\|_2 \cdot \boldsymbol{d}_{\text{def}}$; `// Likely adversarial, enhanced shift`

$y \leftarrow \text{argmax}(\mathcal{H}(\hat{\boldsymbol{f}}))$; `// Compute final prediction`

A.2 IMPLEMENTATION DETAILS

Transformations. In our experiments, DBD applies $n = 31$ transformations per input, yielding 32 images including the original. We provide more details on various image transformations used in DBD in Table 7. (1) For *spatial domain transformations*, each transformation includes random cropping, scaling, and flipping. Due to the stochastic nature of these operations, we perform 16 transformations per input. (2) For *pixel domain transformations*, we implement bit-depth reduction, compressing the original 8-bit image to 3 bits using three quantization methods: `floor`, `round`, and `ceil`. In addition, we apply JPEG compression-decompression with three quality levels (50, 60, 75) to increase diversity. Random Gaussian noise with amplitude $\gamma = 0.1$ is also added, with six stochastic realizations per input. (3) For *frequency domain transformations*, we apply Gaussian, mean, and median filtering with kernel size 5.

In the ablation study (Table 6 and Fig. 4), the resulting average features from Random Crop-Resize-Flip (16 transformations), Bit-depth Reduction (3 operations), JPEG Compression (3 operations), Gaussian Noise (6 operations), and Image Filtering (3 filters) are used for classification.

Text Prompts. For text prompts, we use a mix of hand-crafted prompts and GPT-3-generated prompts provided by CuPL (Pratt et al., 2023), and average text features over multiple prompts per class.

Attacks. All attacks are implemented using the torchattack (Kim, 2020) library. For PGD and FGSM attacks, we follow the baseline R-TPT (Sheng et al., 2025) configuration by using cross-entropy loss in untargeted mode. For the CW attack (Carlini & Wagner, 2017), we use a learning rate of 0.01 with the Adam optimizer. For AutoAttack (AA, (Croce & Hein, 2020b)), we use the standard mode, which includes four components: untargeted APGD-CE (1 restart), targeted APGD-DLR (10 target classes), targeted FAB (10 target classes, (Croce & Hein, 2020a)), and Square Attack (5000 queries, (Andriushchenko et al., 2020)). To remain consistent with the baseline setup, EOT was not applied. When verifying these 4 components, we keep the parameters unchanged.

Table 7: Details of image transformations used in DBD.

Domain	**Transformations**
Spatial	Random cropping-scaling-flipping (16 times)
Pixel	Bit-depth compression (quantization): `floor, round, ceil` (bits = 3) JPEG compression-decompression: `quality = 50, 60, 75` Add Gaussian noise: $\gamma = 0.1$ (6 times)
Frequency	Gaussian filter: `kernel_size = 5` Mean filter: `kernel_size = 5` Median filter: `kernel_size = 5`

A.3 DATASETS

We evaluate our method on 10 fine-grained classification datasets and 5 ImageNet-OOD datasets. Table 8 summarizes their detailed information, including their content, number of categories, number of images and corresponding hand-crafted prompt.

Table 8: Introduction of all datasets involved in experiments.

Dataset	Description	# Classes	# Test	Hand-crafted Prompt
Caltech101	Object images	100	2,465	a photo of a [CLASS]
Pets	Pet images	37	3,669	a photo of a [CLASS], a type of pet
Cars	Car images	196	8,041	a photo of a [CLASS]
Flower102	Flower images	102	2,463	a photo of a [CLASS], a type of flower
Aircraft	Aircraft images	100	3,333	a photo of a [CLASS], a type of aircraft
DTD	Describable textures images	47	1,692	[CLASS] texture
EuroSAT	Sentinel-2 satellite images	10	8,100	a centered satellite photo of a [CLASS]
UCF101	Human action images	101	3,783	a photo of a person doing [CLASS]
SUN397	Scene recognition images	397	19,850	a photo of a [CLASS]
Food101	Food images	101	30,300	a photo of a [CLASS], a type of food
ImageNet	Object and scene images	1,000	50,000	a photo of a [CLASS]
ImageNet-A	Adversarially filtered images	200	7,500	a photo of a [CLASS]
ImageNet-V2	New test images	1,000	10,000	a photo of a [CLASS]
ImageNet-R	Rendered images	200	30,000	a photo of a [CLASS]
ImageNet-S	Sketch-style images	1,000	50,889	a photo of a [CLASS]

A.4 EXPERIMENTS

Detailed results under PGD attack with pseudo-label. Due to space constraints, Table 3 in the main text reports only a subset of the results. Here we provide the complete version in Table 9, which includes results on six fine-grained datasets and three attack settings.

Detailed results under various attacks. We evaluate DBD and baseline methods under additional adversarial attacks, including FGSM (Goodfellow et al., 2014), CW (Carlini & Wagner, 2017), and AutoAttack (AA) (Croce & Hein, 2020b). AA is a stronger, ensemble-based attack that combines targeted FAB (Croce & Hein, 2020a), Square Attack (Andriushchenko et al., 2020), untargeted

Table 9: robust accuracy (%) under three PGD attack settings using **pseudo-labels** on six fine-grained datasets.

Attack & Model	Method	Caltech101	Pets	Flower102	Aircraft	DTD	UCF101	Avg.
Clean		89.1	85.0	65.9	19.6	48.5	59.7	61.3
PGD-100 ($\epsilon = 1/255$) on CLIP-ResNet50	CLIP	7.5	5.6	6.4	1.6	8.2	6.3	5.9
	R-TPT	81.7	77.7	53.2	15.1	35.6	54.3	52.9
	DBD	88.8	82.4	64.4	16.9	47.5	59.0	59.8
Clean		93.3	86.6	67.0	20.6	49.9	63.6	63.5
PGD-100 ($\epsilon = 1/255$) on CLIP-ViT-B/32	CLIP	2.3	3.4	3.8	0.8	3.8	4.9	3.2
	R-TPT	79.9	62.7	43.1	13.9	32.9	49.9	47.1
	DBD	93.0	84.4	66.1	19.5	49.5	62.7	62.5
Clean		94.2	90.3	73.0	27.2	53.2	67.0	67.5
PGD-100 ($\epsilon = 1/255$) on CLIP-ViT-B/16	CLIP	1.7	3.1	2.7	1.5	4.2	4.5	2.9
	R-TPT	84.1	66.1	49.8	18.2	37.1	52.7	51.3
	DBD	94.1	88.6	72.3	26.3	53.1	66.5	66.8

Table 10: Results (%) of clean accuracy (Acc.) and robust accuracy (Rob.) of various attacks on six fine-grained classification datasets.

Method	Caltech101			Pets			Flower102			Aircraft			DTD			UCF101			Avg.		
	CLIP	R-TPT	DBD	CLIP	R-TPT	DBD	CLIP	R-TPT	DBD	CLIP	R-TPT	DBD	CLIP	R-TPT	DBD	CLIP	R-TPT	DBD	CLIP	R-TPT	DBD
Attacks on CLIP-ResNet50																					
FGSM	49.6	79.2	94.2	11.1	72.1	91.1	6.2	49.3	80.8	0.3	12.1	38.2	16.6	33.3	72.0	13.9	48.0	77.2	16.3	49.0	75.6
CW	5.1	79.6	90.6	0.8	74.7	86.6	0.9	51.2	65.6	0.9	14.9	18.8	2.2	33.7	50.1	2.4	51.5	62.0	2.1	50.9	62.3
AA	0.9	81.0	91.4	0.0	76.8	86.0	0.0	53.3	67.6	0.0	15.2	21.1	0.4	35.2	52.2	0.0	53.6	64.6	0.2	52.5	63.8
FAB	33.8	81.8	90.5	1.9	78.7	86.3	1.0	54.8	64.5	0.0	15.2	18.7	10.2	36.3	49.6	8.3	54.4	62.2	9.2	53.5	62.0
Square	50.5	83.2	87.7	36.5	80.4	83.1	33.7	57.7	56.5	1.2	15.8	15.6	19.6	37.3	44.4	18.1	56.7	56.3	26.6	55.2	57.3
APGD-CE	2.7	81.0	91.4	0.0	76.8	85.9	0.0	53.2	67.6	0.0	15.2	21.0	0.7	35.0	52.3	0.0	53.5	64.6	0.6	52.5	63.8
APGD-DLR	1.2	82.1	91.3	0.0	79.0	87.3	0.0	55.3	66.4	0.0	15.4	19.0	0.2	35.8	51.7	0.1	54.4	64.1	0.3	53.6	63.3
Attacks on CLIP-ViT-B/32																					
FGSM	47.2	75.1	87.9	7.1	49.8	88.0	3.7	37.1	69.1	0.2	8.4	36.0	12.9	27.6	51.0	9.7	40.7	61.0	13.5	39.8	65.5
CW	3.0	84.7	92.8	0.4	73.9	87.5	0.9	55.3	69.1	0.2	16.8	22.9	1.5	36.4	50.7	1.4	55.9	64.8	1.2	53.8	64.6
AA	0.4	75.3	93.1	0.0	51.9	87.7	0.0	39.2	69.9	0.0	14.0	24.3	0.0	32.0	52.8	0.0	46.7	67.1	0.1	43.2	65.8
FAB	46.5	87.8	93.5	17.9	78.8	88.1	17.5	58.8	69.3	0.8	17.4	22.4	14.3	39.3	52.2	16.3	59.1	66.0	18.9	56.9	65.3
Square	22.7	86.7	92.2	8.0	77.6	84.7	8.9	57.9	65.6	0.5	17.0	20.4	3.8	37.4	48.3	6.9	58.9	64.0	8.4	55.9	62.5
APGD-CE	1.1	75.3	93.1	0.0	51.9	87.7	0.0	39.2	69.9	0.0	14.0	24.3	0.0	32.0	52.8	0.0	46.7	67.1	0.2	43.2	65.8
APGD-DLR	0.6	79.6	92.3	0.0	60.0	87.1	0.0	46.4	68.8	0.0	14.8	22.7	0.0	33.6	51.5	0.0	50.3	64.8	0.1	47.4	64.5
Attacks on CLIP-ViT-B/16																					
FGSM	47.2	75.6	92.8	7.1	47.9	95.3	3.7	35.3	80.5	0.2	10.1	53.5	12.9	29.4	61.5	9.7	35.1	67.8	13.5	38.9	75.2
CW	3.0	87.3	94.7	0.4	73.4	92.1	0.9	55.7	73.9	0.2	20.0	28.8	1.5	39.5	56.2	1.4	57.4	69.2	1.2	55.6	69.1
AA	0.4	78.9	94.8	0.0	51.2	90.4	0.0	40.6	74.7	0.0	17.3	31.7	0.0	33.7	57.0	0.0	48.2	70.3	0.1	45.0	69.8
FAB	46.5	90.1	95.2	17.9	80.3	92.1	17.5	60.7	74.1	0.8	21.0	28.5	14.3	43.0	56.0	16.3	62.1	69.8	18.9	59.5	69.3
Square	22.7	89.6	93.5	8.0	77.7	87.8	8.9	62.9	68.8	0.5	21.2	24.7	3.8	41.3	50.4	6.9	62.5	65.3	8.4	59.2	65.1
APGD-CE	1.1	78.9	94.8	0.0	51.2	90.4	0.0	40.6	74.7	0.0	17.3	31.7	0.0	33.7	57.0	0.0	48.2	70.3	0.2	45.0	69.8
APGD-DLR	0.6	82.0	94.3	0.0	58.7	91.0	0.0	47.5	73.4	0.0	18.5	30.0	0.0	35.8	55.3	0.0	50.4	67.1	0.1	48.8	68.5

APGD-CE (Auto-PGD with Cross-Entropy loss), and targeted APGD-DLR (Auto-PGD with Difference of Logits Ratio loss), incorporating both gradient-based and gradient-free strategies to comprehensively challenge model robustness. We also separately evaluate defense performance against each of these four constituent attacks. For our DBD, we set $\tau = 0.6$ and $\lambda = 2.5$ (with $\lambda = 5$ for FGSM). We assess the effectiveness of various attacks on six fine-grained datasets across three attack settings, and detailed results are shown in Table 10.

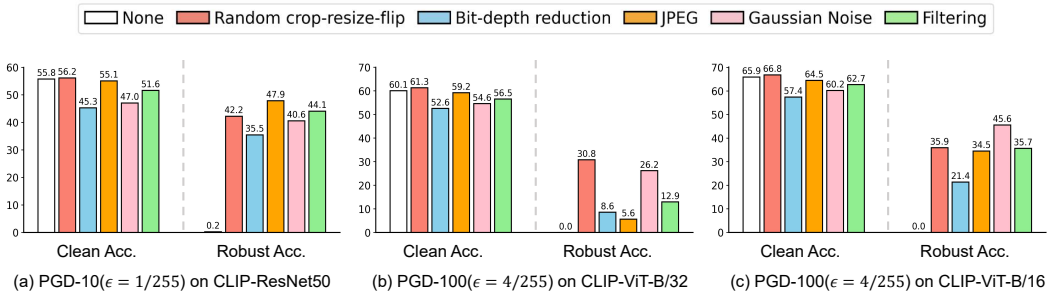

(a) PGD-10($\epsilon = 1/255$) on CLIP-ResNet50 (b) PGD-100($\epsilon = 4/255$) on CLIP-ViT-B/32 (c) PGD-100($\epsilon = 4/255$) on CLIP-ViT-B/16

Figure 4: Average results (%) of clean accuracy (Clean Acc.) and robust accuracy (Robust Acc.) for various types of transformations across 15 datasets under three attack settings.

Detailed analysis of various image transformations. We ablate the individual image transformations used in DBD to assess their standalone effects (as Fig.4). JPEG compression-decompression preserves clean accuracy while providing moderate defense against low-strength attacks, though its effectiveness diminishes as attack strength increases. Random crop-resize-flip slightly improves clean accuracy and shows robustness across different attack strengths and model backbones. Adding Gaussian noise can yield strong defense in certain cases but substantially degrades clean accuracy. By combining multiple transformations, DBD leverages their complementary strengths to gener-

ate more reliable features across diverse scenarios and model variants; moreover, integration of transformations mitigates the risk of defenses being circumvented by attacks tailored to a single transformation.

More ablation study on the DB-score threshold τ. We evaluate the detection performance of adversarial examples using the DB-score. Specifically, we assess the effect of threshold τ under three PGD attack settings across 15 datasets, reporting both the mean detection accuracy and mean F1-score averaged over all datasets and attack settings. Results are presented in Fig.5. The results show that $\tau = 0.8$ achieves near-optimal detection performance, and the metric remains stable in its neighborhood. This supports our choice and confirms that the DB-score provides a reliable signal for distinguishing adversarial from clean inputs.

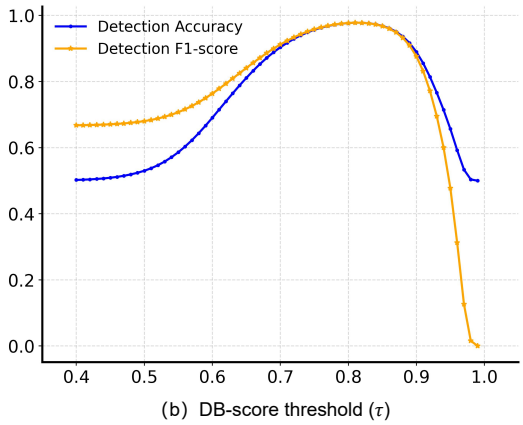

Figure 5: Average results of detection accuracy and F1-score for various types of transformations across 15 datasets under three attack settings.

Geometric Verification of the Proposed Defense Direction. To validate our hypothesis that the Defense Direction genuinely points toward the correct decision region, we conduct a geometric analysis by measuring the cosine similarity between the estimated Defense Direction and two critical reference directions. The first is the *Clean Direction*, defined as the vector from the adversarial image's feature to its corresponding clean (unperturbed) counterpart's feature. The second is the *Class Centroid Direction*, defined as the vector from the adversarial image's feature to the centroid of features belonging to the true class (computed using correctly classified clean images).

Table 11 presents the average cosine similarities across multiple fine-grained datasets under the PGD-100 (ϵ=4/255) attack on CLIP-ViT-B/16. The results demonstrate that our proposed Defense Direction exhibits extremely high similarity (≈ 0.95) with the Clean Direction and substantial similarity (≈ 0.90) with the Class Centroid Direction. These high cosine similarities provide strong geometric evidence that the Defense Direction indeed aligns closely with both the clean feature direction and the correct class centroid, supporting our hypothesis that the Defense Direction points back toward the correct decision region.

Table 11: Average cosine similarity between Defense Direction and reference directions across datasets under PGD-100($\epsilon = 4/255$) attack on CLIP-ViT-B/16.

Reference Direction	Pets	Caltech101	Food101	Cars	ImageNet
Clean Direction	0.957	0.945	0.939	0.943	0.951
Class Centroid Direction	0.932	0.917	0.898	0.905	0.892

Adaptive Attack with BPDA and EOT. While our primary evaluation based on the threat model described in Section 3.1, we additionally evaluate against adaptive, defense-aware attacks to assess potential vulnerabilities. Based on PGD attack, we implement BPDA (Backward Pass Differentiable Approximation, Athalye et al. (2018)) combined with EOT (Expectation Over Transformation, (Xie et al., 2017)) to approximate gradients through our differentiable DBD pipeline. During attack

optimization, non-differentiable components are replaced with identity functions in the backward pass, while gradients are averaged over multiple stochastic forward passes.

We evaluate on Caltech101 dataset using strong adaptive attacks: PGD-10 (ϵ=1/255) against CLIP-ResNet50 and PGD-100 (ϵ=4/255) against CLIP-ViT-B/16. Results in Table 12 show that when attackers explicitly optimize through the full DBD pipeline, robust accuracy degrades significantly (to 50.79% and 1.29%, respectively). Notably, these adversarial images generated buy adaptive attacks also perform substantially worse against the original CLIP model compared to standard attacks, suggesting overfitting to the defense mechanism.

Critically, under the adaptive attack (PGD-100), the average DB-score remains high (0.89), with approximately 81% of adversarial samples exceeding our detection threshold (τ=0.80). This reveals an important insight: *the directional bias pattern persists under adaptive attacks, but the estimated direction is manipulated to point away from the true class*. In other words, while adaptive attacks can subvert the defense functionality by distorting the Defense Direction, they cannot eliminate the underlying directional bias signal—making such attacks still detectable through our DB-score metric.

Table 12: Robust accuracy (%) under adaptive attacks with BPDA+EOT on Caltech101.

Attacks	**Original CLIP**	**CLIP with DBD**
PGD-10 (ϵ=1/255)	84.26	50.79
PGD-100 (ϵ=4/255)	81.05	1.29

A.5 Use of LLMs

In this work, we used ChatGPT to assist in polishing the writing of this paper, focusing primarily on improving clarity, grammar, and style. The model was not involved in the generation of ideas or experimental designs. All the concepts, analyses, and conclusions presented are entirely our own.